

Are your MRI contrast agents cost-effective?

Learn more about generic Gadolinium-Based Contrast Agents.



**FRESENIUS
KABI**

caring for life

AJNR

This information is current as
of April 17, 2024.

**Material-Specific Roadmap Modes Can
Improve the Visibility of Liquid Embolic
Agents for Endovascular Embolization: A
Systematic In Vitro Study**










N. Schmitt, L. Wucherpfennig, S. Hohenstatt, K.
Karimian-Jazi, M.O. Breckwoldt, H.-U. Kauczor, M.
Bendszus, M.A. Möhlenbruch and D.F. Vollherbst

AJNR Am J Neuroradiol 2022, 43 (12) 1749-1755

doi: <https://doi.org/10.3174/ajnr.A7706>

<http://www.ajnr.org/content/43/12/1749>

Material-Specific Roadmap Modes Can Improve the Visibility of Liquid Embolic Agents for Endovascular Embolization: A Systematic In Vitro Study

 N. Schmitt,  L. Wucherpfennig,  S. Hohenstatt,  K. Karimian-Jazi,  M.O. Breckwoldt,  H.-U. Kauczor,  M. Bendszus,  M.A. Möhlenbruch, and  D.F. Vollherbst

ABSTRACT

BACKGROUND AND PURPOSE: Endovascular embolization using liquid embolic agents is a safe and effective treatment option for AVMs and fistulas. Because reliable visibility of these liquid embolic agents is essential for intraprocedural visual control to prevent complications, novel angiographic systems are equipped with material-specific roadmap modes. The aim of this study was the systematic in vitro comparison of conventional and material-specific roadmap modes regarding the visibility of the most used liquid embolic agents.

MATERIALS AND METHODS: A recently introduced in vitro model, resembling cerebral vessels, was embolized with Onyx 18, Squid 18, PHIL 25%, and *n*-BCA mixed with iodized oil ($n = 4$ for each liquid embolic agent), as well as with contrast medium and saline, both serving as a reference. Imaging was performed in conventional and material-specific roadmap modes. The visibility of the liquid embolic agents in both modes was compared quantitatively and qualitatively.

RESULTS: Significant differences between conventional and material-specific roadmap modes regarding the visibility of the liquid embolic agents were observed for all study groups. All liquid embolic agents were better visible in the material-specific roadmap modes compared with the conventional mode in qualitative and quantitative analyses (eg, Onyx in conventional-versus-material-specific modes along the 1.0-mm sector: mean contrast-to-noise ratio, 5.69 [SD, 0.85] versus 47.18 [SD, 5.72]; $P < .001$, respectively).

CONCLUSIONS: In this in vitro study, we demonstrated a better visibility of all investigated liquid embolic agents by using material-specific roadmap modes compared with the conventional roadmap technique. Especially in complex anatomic situations, these novel roadmap modes could improve the visual control and thus the safety and efficacy of embolization procedures in clinical practice.

ABBREVIATIONS: CNR = contrast-to-noise ratio; DU = density units; LEA = liquid embolic agent

Endovascular embolization using liquid embolic agents (LEAs) is an effective treatment mode for therapy of cerebral and spinal vascular disorders, such as AVMs or dural AVFs.^{1–6} In recent years, the range of available LEAs, each with different properties, has increased steadily. Onyx (Medtronic), Squid (Balt), and the precipitating hydrophobic injectable liquid (PHIL; MicroVention) represent the most commonly used copolymer-based, nonadhesive LEAs on the market. The embolic agents Onyx and Squid consist of ethylene-vinyl alcohol copolymer, dimethyl-sulfoxide,

and radiopaque tantalum powder, while PHIL consists of 2 specific copolymers (poly[lactide-co-glycolide] and polyhydroxyethylmethacrylate) and covalently bound triiodophenol for intrinsic radio-opacity. Regarding both ethylene-vinyl alcohol copolymer-based LEAs, Squid features a smaller (“micronized”) grain size of the admixed tantalum powder, aiming for a more homogeneous radio-opacity and thus better visibility during longer injection procedures.

Before the introduction of these nonadhesive embolic agents, liquid embolization was primarily performed with cyanoacrylates. With their most frequently used active component being *n*-BCA, cyanoacrylates are still applied frequently, for example, for the therapy of lesions that cannot be reached with dimethyl-sulfoxide-compatible catheters or for embolization of high-flow shunts in AVMs or dural AVFs. *n*-BCA and its derivatives are normally mixed with iodized oil (ratio 1:1; Lipiodol Ultra Fluid; Guerbet) to enable sufficient visibility.⁷ During embolization procedures, a reliable visibility of the embolic material is essential for

Received August 18, 2022; accepted after revision October 12.

From the Departments of Neuroradiology (N.S., S.H., K.K.-J., M.O.B., M.B., M.A.M., D.F.V.) and Diagnostic and Interventional Radiology (L.W., H.-U.K.), Heidelberg University Hospital, Heidelberg, Germany.

N. Schmitt and L. Wucherpfennig contributed equally to this work.

Please address correspondence to Dominik F. Vollherbst, MD, Department of Neuroradiology, Heidelberg University Hospital, INF 400, 69120 Heidelberg, Germany; e-mail: Dominik.Vollherbst@med.uni-heidelberg.de

<http://dx.doi.org/10.3174/ajnr.A7706>

visual control and to prevent possible complications, for example embolization of AVM-related draining veins or inadvertent embolization of vessels supplying healthy brain tissue. Therefore, the novel angiographic system Artis icono (Siemens Healthineers) is equipped with material-specific roadmap modes aimed at improving the visualization of LEAs. As described recently, the technical principle of these modes is based on a contrast-to-noise ratio (CNR)-driven exposure control, which adjusts the imaging setting of the angiography suite automatically and thereby optimizes image quality, while reducing the radiation dose at the same time.^{8,9}

To date, there is only 1 experimental study available investigating and comparing the visibility of different LEAs, while the potential of material-specific roadmap modes has not been investigated so far.¹⁰ The aim of the present study was the systematic in vitro comparison of conventional and material-specific roadmap techniques regarding the visibility of the most used LEAs.

MATERIALS AND METHODS

Sample Preparation

A recently introduced in vitro model was used for the present study, consisting of connected sectors with different diameters, ranging from 2.0 to 0.5 mm, and manufactured using a 3D printer, consisting of the biocompatible synthetic material VisiJet.¹⁰ Each in vitro model ($n = 4$ per LEA, contrast medium, and saline) was embolized by a manual pulsatile LEA injection using a standard embolization microcatheter (SONIC 1.2F, 35-mm detachable tip length; Balt) as well as 1-mL, dimethyl-sulfoxide-compatible syringes. Moreover, during the embolization procedure, there was a continuous flush of saline (NaCl 0.9%) with a flow of 60 mL per hour. All LEAs were prepared in accordance with the manufacturer's instructions and as recommended for clinical use. Embolization of the in vitro models was performed for the following LEAs: Onyx 18, Squid 18, PHIL 25%, *n*-BCA mixed with iodized oil as well as contrast medium (iopamidol, Imeron 300; Bracco) and NaCl 0.9%.

An exemplary image of an in vitro model embolized with Onyx is provided in Fig 1.

Imaging

Roadmap imaging was performed using the Artis icono angiography suite (Siemens Healthineers). A pulsed imaging mode with a pulse rate of 7.5 p/s was used, and images were acquired with standard settings according to clinical routine in a conventional (for all investigated LEAs, contrast medium, and saline) as well as a material-specific roadmap mode (tantalum-specific mode for Onyx and Squid; iodine-specific mode for PHIL and *n*-BCA mixed with iodized oil and contrast medium). The FOV of the receptor was 25 cm. Further acquisition settings, such as the tube parameters, collimations settings, and source-image distance, were adjusted automatically by the image-quality system OPTIQ (Siemens Healthineers).

Quantitative Analysis

Quantitative image analysis comparing the visibility of LEAs in a conventional and material-specific roadmap mode was performed on a PACS workstation. Five similar rectangular ROIs with a length of 4 mm and widths similar to the diameter of the cylindrical cavity (2.0, 1.5, 1.5, and 0.5 mm, respectively) were drawn manually

along each sector of the in vitro models. Because the sector of the smallest cavity (0.5 mm) features a length of 30 mm, the ROIs were drawn along its proximal part. For each ROI, the mean density units (DU) were calculated. Simultaneously, 5 square ROIs (side length: 4 mm) were drawn in proximity on a similar level on the noncavity part of each in vitro model. For the ROIs on the noncavity part, the mean background DU and their corresponding SDs were calculated. Each ROI drawing was performed in consensus with a neuroradiology resident and a neuroradiology attending physician (6 and 9 years' experience in diagnostic imaging) and was for the conventional as well as the material-specific roadmap images. Afterward, the CNR was calculated for each level of the in vitro models using the following formula:¹¹

$$CNR = \frac{|\text{Mean DU}_{LEA} - \text{Mean DU}_{background}|}{SD_{background}}$$

Qualitative Image Analysis

Qualitative image analysis of the conventional and material-specific roadmap images was performed by 2 different readers (both with 6 years' experience in diagnostic imaging) on a PACS workstation. A second read was performed after 12 weeks to improve the quality of the qualitative analysis. Both readers were blinded to the type of roadmap mode as well as to the type of LEA, contrast medium, and saline. All window settings were left as predetermined by the angiography suite with a window width of 4095 DU and a level of 2047 DU, while a manual adjustment of the window settings was not allowed. The visibility of each LEA, contrast medium, and saline along each sector (diameters of 2.0, 1.5, 1.0, and 0.5 mm, respectively) was graded by a 5-point scale: 1) no visibility, 2) poor visibility, 3) acceptable visibility, 4) good visibility, and 5) excellent visibility. The grading was performed for both the conventional and material-specific roadmap modes, except saline for which images were only acquired and analyzed in conventional mode.

Statistics

GraphPad Prism (Version 9.3.1; GraphPad Software) was used for statistical analysis. The interreader and intrareader agreement were assessed with the Cohen κ coefficient. The κ values were interpreted as follows: ≤ 0.20 , poor agreement; 0.21–0.40, fair agreement; 0.41–0.60, moderate agreement; 0.61–0.80, good agreement; and 0.81–1.00, very good agreement.^{12,13} To evaluate statistical differences between the conventional and the material-specific roadmap modes regarding the visibility of the different LEAs, we performed the Mann-Whitney *U* test. There was no statistical testing for the control groups (contrast medium and saline) because they only served as a reference. The results of the quantitative analysis are presented as mean CNR (SD), and of the qualitative analysis as the mean score. The level of statistical significance was defined as $P < .05$.

RESULTS

Illustrations of the roadmap images in conventional and material-specific modes are demonstrated in Fig 1. The results of the quantitative and qualitative image analyses are summarized in Fig 2.

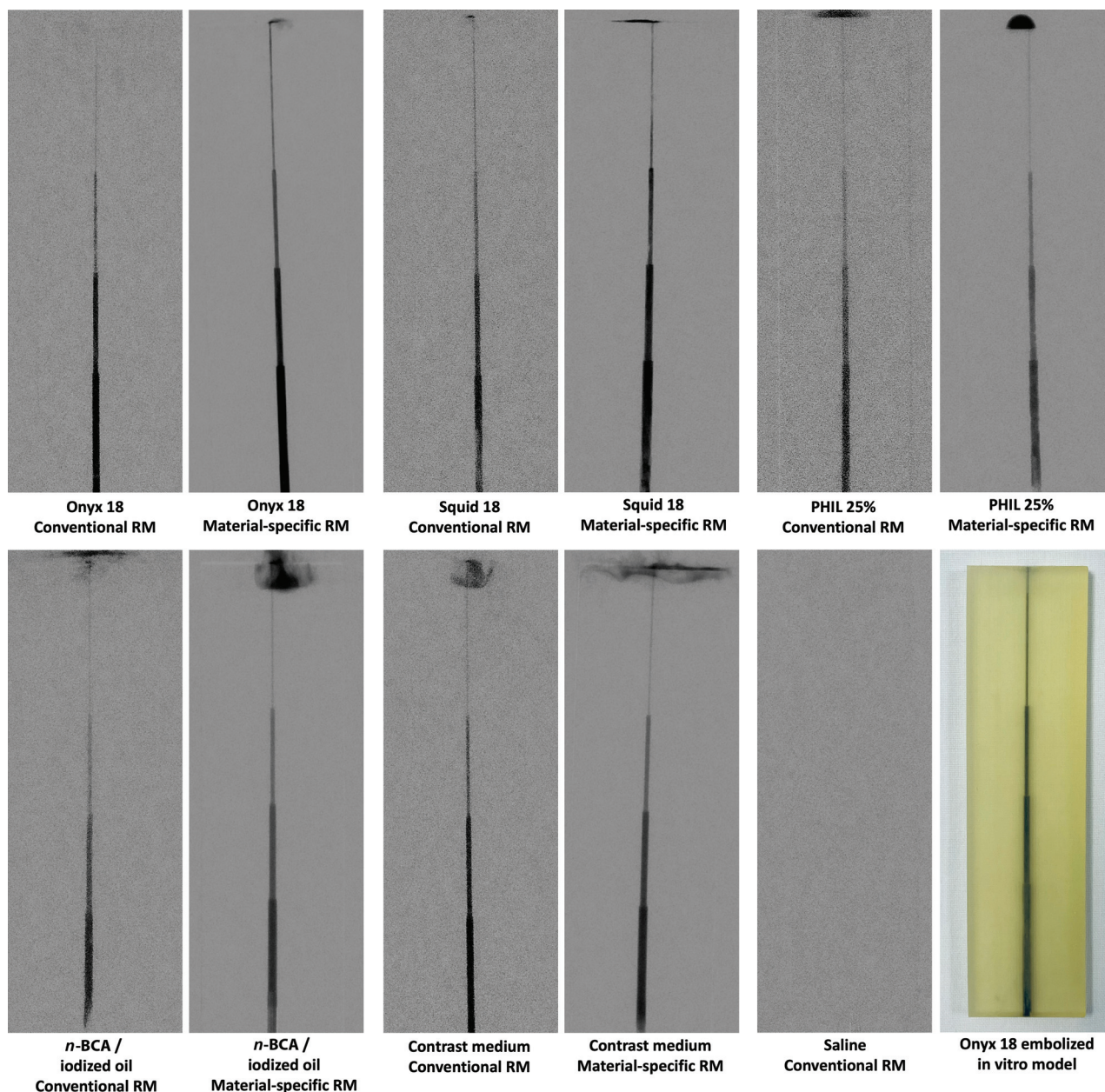


FIG 1. Representative images of the in vitro models embolized with different LEAs as well as contrast medium and saline, both serving as a reference. The images in the conventional and material-specific roadmap techniques are illustrated next to each other (left: conventional roadmap mode; right: material-specific roadmap mode) for each investigated LEA. The window width was set at 4095 DU, and the window level at 2047 DU. An exemplary image of an Onyx-embolized in vitro model is provided in the lower row as well. Please note the radiopaque embolic material at the upper end of most embolized models, which is of artificial character and had no influence on the present results. RM indicates roadmap mode.

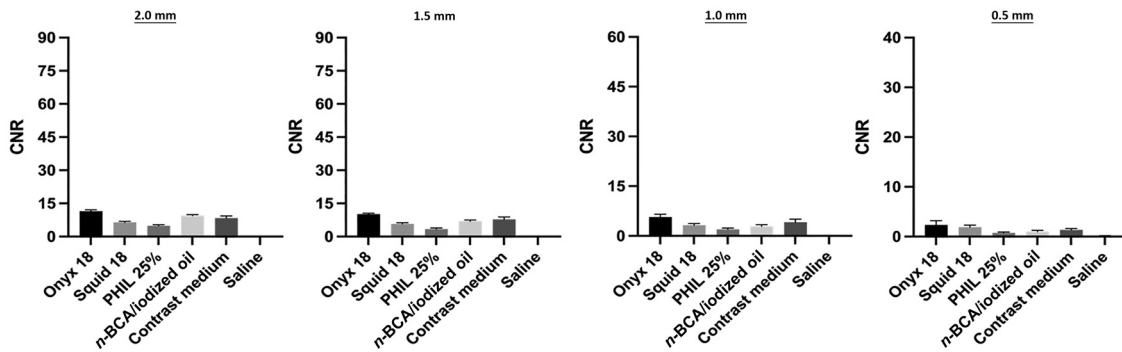
Along all sectors of the in vitro model (2.0, 1.5, 1.0, and 0.5 mm), quantitative results demonstrated a significant difference ($P < .001$, respectively) among the CNRs of the investigated LEAs and thus a better visibility in the material-specific roadmap mode compared with the conventional roadmap mode (for example, Onyx 18 in conventional-versus-material-specific roadmap mode along all investigated diameters [mean CNR], 2.0 mm: 11.53 [SD, 0.57] versus 77.09 [SD, 3.23]; 1.5 mm: 10.17 [SD, 0.44] versus 66.06 [SD, 5.97]; 1.0 mm: 5.69 [SD, 0.85] versus 47.18 [SD, 5.72]; and 0.5 mm: 2.36 [SD, 0.83] versus 30.27 [SD, 6.78]; $P < .001$, respectively). Detailed information on the CNR values of the

investigated LEAs as well as the control groups (contrast medium and saline) are provided in [Table 1](#).

The interreader reliability ($\kappa = 0.821$; range, 0.774–0.868) as well as the intrareader reliability ($\kappa = 0.862$; range, 0.820–0.904) both demonstrated very good agreement for the qualitative analysis of the roadmap images by both readers.

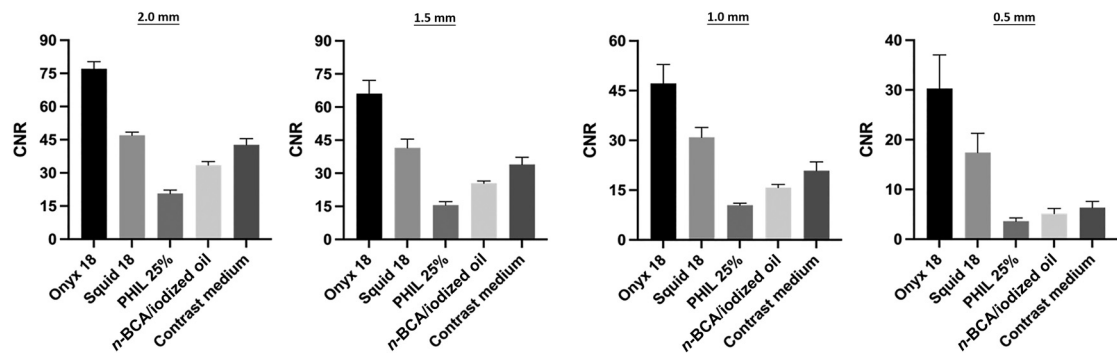
Compared with the quantitative results, the qualitative scores demonstrated similar findings. There was a higher score and thus better visibility of all investigated LEAs along each sector of the in vitro model ($P < .02$, respectively; for example, PHIL 25% in conventional-versus-material-specific roadmap mode [mean score],

Quantitative analyses: Conventional Roadmap



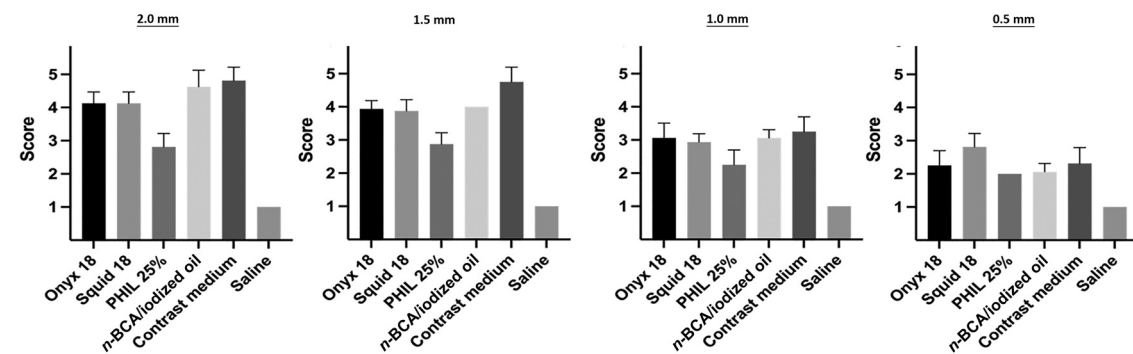
A

Quantitative analyses: Material-specific Roadmap



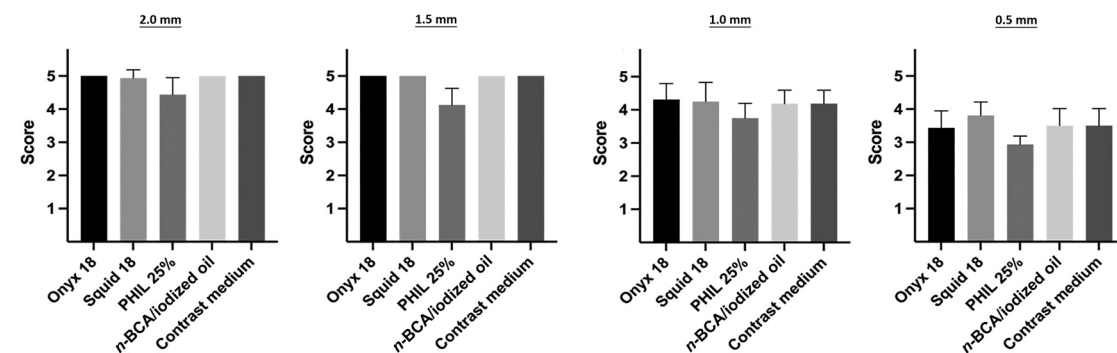
B

Qualitative analyses: Conventional Roadmap



C

Qualitative analyses: Material-specific Roadmap



D

FIG 2. Results of the quantitative (A and B) and qualitative (C and D) analyses of the conventional and the material-specific roadmap images regarding the visibility of the different LEAs, contrast medium and saline, both serving as a reference. Material-specific roadmap images demonstrate an improved visibility of the different LEAs compared with the conventional roadmap technique along all sectors of the in vitro model (2.0, 1.5, 1.0, and 0.5 mm; $P < .05$, respectively). Roadmap images of saline were acquired only in conventional roadmap mode because there is no material-specific mode available.

Table 1: Summary of the results of the quantitative analysis^a

LEA	Conventional Roadmap	Material-Specific Roadmap	P Value
2.0 mm			
Onyx 18	11.53 (SD, 0.57)	77.09 (SD, 3.23)	$P < .001$
Squid 18	6.43 (SD, 0.40)	46.97 (SD, 1.42)	$P < .001$
PHIL 25%	4.91 (SD, 0.47)	20.69 (SD, 1.51)	$P < .001$
<i>n</i> -BCA/iodized oil	9.50 (SD, 0.42)	33.46 (SD, 1.66)	$P < .001$
Contrast medium	8.39 (SD, 0.96)	42.72 (SD, 2.76)	NA
Saline	0.08 (SD, 0.06)	NA	
1.5 mm			
Onyx 18	10.17 (SD, 0.44)	66.06 (SD, 5.97)	$P < .001$
Squid 18	5.77 (SD, 0.50)	41.52 (SD, 4.00)	$P < .001$
PHIL 25%	3.41 (SD, 0.52)	15.54 (SD, 1.63)	$P < .001$
<i>n</i> -BCA/iodized oil	6.96 (SD, 0.46)	25.44 (SD, 1.06)	$P < .001$
Contrast medium	7.75 (SD, 1.17)	34.01 (SD, 3.21)	NA
Saline	0.06 (SD, 0.03)	NA	
1.0 mm			
Onyx 18	5.69 (SD, 0.85)	47.18 (SD, 5.72)	$P < .001$
Squid 18	3.20 (SD, 0.53)	30.92 (SD, 3.00)	$P < .001$
PHIL 25%	1.97 (SD, 0.39)	10.47 (SD, 0.62)	$P < .001$
<i>n</i> -BCA/iodized oil	2.86 (SD, 0.52)	15.77 (SD, 0.94)	$P < .001$
Contrast medium	4.12 (SD, 0.89)	20.88 (SD, 2.64)	NA
Saline	0.10 (SD, 0.07)	NA	
0.5 mm			
Onyx 18	2.36 (SD, 0.83)	30.27 (SD, 6.78)	$P < .001$
Squid 18	1.91 (SD, 0.42)	17.40 (SD, 3.89)	$P < .001$
PHIL 25%	0.733 (SD, 0.19)	3.61 (SD, 0.67)	$P < .001$
<i>n</i> -BCA/iodized oil	0.97 (SD, 0.28)	5.16 (SD, 1.01)	$P < .001$
Contrast medium	1.34 (SD, 0.28)	6.35 (SD, 1.27)	NA
Saline	0.14 (SD, 0.06)	NA	

Note:—NA indicates that no *P* value is available because the contrast medium and saline only served as a reference with no material-specific roadmap mode available for saline.

^aResults are mean CNR.

Table 2: Summary of the results of the qualitative analysis^a

LEA	Conventional Roadmap	Material-Specific Roadmap	P Value
2.0 mm			
Onyx 18	4.13 (SD, 0.34)	5.00 (SD, 0.00)	$P < .001$
Squid 18	4.13 (SD, 0.34)	4.94 (SD, 0.25)	$P < .001$
PHIL 25%	2.81 (SD, 0.40)	4.44 (SD, 0.51)	$P < .001$
<i>n</i> -BCA/iodized oil	4.63 (SD, 0.50)	5.00 (SD, 0.00)	$P = .018$
Contrast medium	4.81 (SD, 0.40)	5.00 (SD, 0.00)	NA
Saline	1.00 (SD, 0.00)	NA	
1.5 mm			
Onyx 18	3.94 (SD, 0.25)	5.00 (SD, 0.00)	$P < .001$
Squid 18	3.88 (SD, 0.34)	5.00 (SD, 0.00)	$P < .001$
PHIL 25%	2.88 (SD, 0.34)	4.13 (SD, 0.50)	$P < .001$
<i>n</i> -BCA/iodized oil	4.00 (SD, 0.00)	5.00 (SD, 0.00)	$P < .001$
Contrast medium	4.75 (SD, 0.45)	5.00 (SD, 0.00)	NA
Saline	1.00 (SD, 0.00)	NA	
1.0 mm			
Onyx 18	3.06 (SD, 0.44)	4.31 (SD, 0.48)	$P < .001$
Squid 18	2.94 (SD, 0.25)	4.25 (SD, 0.58)	$P < .001$
PHIL 25%	2.25 (SD, 0.45)	3.75 (SD, 0.45)	$P < .001$
<i>n</i> -BCA/iodized oil	3.06 (SD, 0.25)	4.14 (SD, 0.34)	$P < .001$
Contrast medium	3.25 (SD, 0.45)	4.19 (SD, 0.40)	NA
Saline	1.00 (SD, 0.00)	NA	
0.5 mm			
Onyx 18	2.25 (SD, 0.45)	3.44 (SD, 0.51)	$P < .001$
Squid 18	2.81 (SD, 0.40)	3.81 (SD, 0.40)	$P < .001$
PHIL 25%	2.00 (SD, 0.00)	2.94 (SD, 0.25)	$P < .001$
<i>n</i> -BCA/iodized oil	2.06 (SD, 0.25)	3.94 (SD, 0.25)	$P < .001$
Contrast medium	2.31 (SD, 0.48)	3.50 (SD, 0.52)	NA
Saline	1.00 (SD, 0.00)	NA	

Note:—NA indicates that no *P* value is available because the contrast medium and saline only served as a reference with no material-specific roadmap mode available for saline.

^aResults are mean score.

2.0 mm: 2.81 [SD, 0.40] versus 4.44 [SD, 0.51]; 1.5 mm: 2.88 [SD, 0.34] versus 4.13 [SD, 0.50]; 1.0 mm: 2.25 [SD, 0.45] versus 3.75 [SD, 0.45]; and 0.5 mm: 2.00 [SD, 0.00] versus 2.94 [SD, 0.25]). Further details on the qualitative scores are provided in Table 2.

The automatically adjusted imaging parameters of the angiography suite were set as 40 kV(peak) for conventional as well as tantalum-specific roadmap modes, respectively, and 48 kV(p) for the iodine-specific roadmap mode. The automatically set tube current varied between 51 and 58 mA for the conventional and between 117 and 123 mA for the material-specific roadmap modes (tantalum-specific mode: range, 117–123 mA; iodine-specific mode: range, 118–123 mA).

DISCUSSION

In this in vitro study investigating the most commonly used LEAs for endovascular embolization, material-specific roadmap modes improved the visibility of these agents, both in quantitative and qualitative analyses.

During endovascular embolization procedures, adequate visibility of the embolic agent being used is of great importance. For example, unseen inadvertent embolization of healthy blood vessels can lead to ischemic stroke, and premature embolization of the draining veins of a cerebral AVM has the risk of periprocedural hemorrhage.¹⁴ Especially in complex anatomic situations, potentially aggravated by overlying embolic agents or bony structures and when embolizing very small vessels, the visibility can be impeded despite modern angiography systems. Each LEA that is used in clinical practice uses an admixed or an intrinsic material that causes radiopacity and thus enables the visibility of the embolic agent.⁷ To our knowledge, the Artis icono angiography suite is the only commercially available system that is equipped with material-specific roadmap modes to provide an improved visualization of the embolic material during embolization procedures. The potential of these novel roadmap modes has not been the focus of research until now. Therefore, the present study aimed to compare these material-specific road-

map modes with a conventional roadmap technique regarding the visibility of the most used LEAs. The results of our in vitro study demonstrated an improved visibility of the investigated embolic agents Onyx 18, Squid 18, PHIL 25%, and *n*-BCA mixed with iodized oil (ratio 1:1) in the material-specific roadmap modes (tantalum-specific mode for Onyx and Squid and iodine-specific mode for PHIL and *n*-BCA mixed with iodized oil) compared with the conventional roadmap mode ($P < .02$, respectively).

Today, there is only 1 study available investigating the angiographic visibility of LEAs.¹⁰ Schmitt et al¹⁰ compared the visibility of Onyx 18, Squid 18, Squid 12, PHIL 25%, PHIL LV, and *n*-BCA mixed with iodized oil (ratio 1:1) quantitatively and qualitatively in fluoroscopy. Using the same angiography suite and comparable imaging settings as in the present study, the authors described a better in vitro visibility of the tantalum-based LEAs Onyx and Squid as well as *n*-BCA mixed with iodized oil (ratio 1:1) compared with both triiodophenol-based formulations of PHIL. As a possible reason for their findings, they described the higher atomic number of tantalum (atomic number 73) compared with iodine (atomic number 53). The present study focused on the 4 clinically more frequently used LEAs, Onyx 18, Squid 18, PHIL 25%, and *n*-BCA mixed with iodized oil (ratio 1:1), 2 each containing tantalum and iodine as their radiopaque component. The direct comparison of different LEAs regarding their visibility was not the focus of the present research because this topic was described recently and the roadmap technique is based on postprocessing of fluoroscopy. As mentioned before, both material-specific roadmap modes of the Artis icono angiography suite demonstrated an enhanced visibility of the embolic agents compared with the conventional roadmap technique in both analyses. As a possible reason for the present results, we found the individual imaging settings that were adjusted automatically by the image-quality system OPTIQ of the Artis icono angiography suite. In this context, the kV (peak) for the conventional as well as the tantalum-specific roadmap mode was 40 kV(p), respectively, and 48 kV(p) for the iodine-specific roadmap mode. Furthermore, the tube current varied between 51 and 58 mA for the conventional and between 117 and 123 mA for the material-specific roadmap modes (tantalum-specific mode: range, 117–123 mA; iodine-specific mode: range, 118–123 mA) in our in vitro study.

Compared with the conventional roadmap technique, the increased tube voltage and tube current of the material-specific roadmap modes generate an increased quality and quantity of x-radiation. These automatically adjusted settings in combination with the automated, CNR-based adaption of the copper filter of the angiography suite may result in a hardening of the x-ray beam and thus optimize the visibility of the high atomic LEAs in the material-specific roadmap modes compared with the conventional roadmap technique. Two preclinical studies by Dehairs et al⁸ and Werncke et al⁹ further described the potential of a substantial dose reduction with this innovation, which is especially relevant for prolonged embolization procedures, embolization in younger patients, or the inclusion of the eye lens in the FOV. However, the present study focused on the in vitro comparison of material-specific and conventional roadmap modes regarding the visibility of the most used LEAs. Moreover, an additional measurement of the radiation dose was not possible because further test images in different positions of the in vitro model as well

as fluoroscopic images were acquired throughout this study, impeding an adequate comparability among the study groups. The impact of material-specific and conventional roadmap modes on the radiation dose is of great importance and needs to be investigated in a clinical setting in future studies.

This study has several limitations. In general, the transferability of in vitro roadmap imaging to clinical roadmap imaging is limited. Especially, the imaging settings of the angiography suite, which were set automatically, might differ substantially in clinical routine due to the distinct density of the human skull and soft tissues. Moreover, the properties of the LEAs relate closely to the physical properties of blood, such as the concentration of electrolytes, the pH value, or the body temperature; thus, a different visibility of the embolic agents might be possible. Only 4 samples per LEA as well as 1 mixture of *n*-BCA mixed with iodized oil (ratio 1:1) were investigated, mainly explained by the high expenses of the LEAs and the in vitro models used.

CONCLUSIONS

In this in vitro study, the potential of material-specific roadmap modes of the Artis icono angiography suite was compared with the conventional roadmap technique regarding the visibility of LEAs for embolization of vascular malformations. Quantitative and qualitative analyses showed a better visibility of all investigated LEAs (Onyx 18, Squid 18, PHIL 25%, and *n*-BCA mixed with iodized oil [ratio 1:1]) in the material-specific roadmap modes. Especially in complex anatomic situations, these novel roadmap modes could improve the visual control and thus the safety and efficacy of embolization procedures in clinical practice.

Disclosure forms provided by the authors are available with the full text and PDF of this article at www.ajnr.org.

REFERENCES

1. Gross BA, Du R. **Diagnosis and treatment of vascular malformations of the brain.** *Curr Treat Options Neurol* 2014;16:279 [CrossRef Medline](#)
2. Friedlander RM. **Clinical practice: arteriovenous malformations of the brain.** *N Engl J Med* 2007;356:2704–12 [CrossRef Medline](#)
3. Chen CJ, Ding D, Derdeyn CP, et al. **Brain arteriovenous malformations: a review of natural history, pathobiology, and interventions.** *Neurology* 2020;95:917–27 [CrossRef Medline](#)
4. Wu EM, El Ahmadieh TY, McDougall CM, et al. **Embolization of brain arteriovenous malformations with intent to cure: a systematic review.** *J Neurosurg* 2019;132:388–99 [CrossRef Medline](#)
5. Gross BA, Albuquerque FC, Moon K, et al. **Evolution of treatment and a detailed analysis of occlusion, recurrence, and clinical outcomes in an endovascular library of 260 dural arteriovenous fistulas.** *J Neurosurg* 2017;126:1884–93 [CrossRef Medline](#)
6. Patsalides A, Knopman J, Santillan A, et al. **Endovascular treatment of spinal arteriovenous lesions: beyond the dural fistula.** *AJNR Am J Neuroradiol* 2011;32:798–808 [CrossRef Medline](#)
7. Vollherbst DF, Chapot R, Bendszus M, et al. **Glue, Onyx, Squid or PHIL? Liquid embolic agents for the embolization of cerebral arteriovenous malformations and dural arteriovenous fistulas.** *Clin Neuroradiol* 2022;32:25–38 [CrossRef](#)
8. Dehairs M, Bosmans H, Marshall NW. **Implementation of a spatio-temporal figure of merit for new automatic dose rate control regimes in dynamic x-ray imaging.** *Phys Med Biol* 2019;64:045001 [CrossRef Medline](#)
9. Werncke T, Kemling M, Tashenov S, et al. **Impact of a contrast-to-noise ratio driven and material specific exposure control on image**

- quality and radiation exposure in angiography. *Phys Med Biol* 2021;66:065020 [CrossRef Medline](#)
10. Schmitt N, Wucherpfennig L, Hohenstatt S, et al. **Visibility of liquid embolic agents in fluoroscopy: a systematic in vitro study.** *J Neurointerv Surg* 2022;4:018958 [CrossRef Medline](#)
 11. Goode AR, Snyder C, Snyder A, et al. **Signal and contrast to noise ratio evaluation of fluoroscopic loops for interventional fluoroscope quality control.** *J Appl Clin Med Phys* 2019;20:172–80 [CrossRef Medline](#)
 12. Altman DG. *Practical Statistics for Medical Research*. CRC Press; 1990
 13. Cohen J. **A coefficient of agreement for nominal scales.** *Educ Psychol Meas* 1960;20:37–46 [CrossRef](#)
 14. Derdeyn CP, Zipfel GJ, Albuquerque FC, et al; American Heart Association Stroke Council. **Management of Brain Arteriovenous Malformations: A Scientific Statement for Healthcare Professionals From the American Heart Association/American Stroke Association.** *Stroke* 2017;48:e200–24 [CrossRef Medline](#)